IMMUNOLOGY

Affinity maturation of antibody responses is mediated by differential plasma cell proliferation

Andrew J. MacLean[1]*, Lachlan P. Deimel[1], Pengcheng Zhou[1], Mohamed A. ElTanbouly[1], Julia Merkenschlager[1]†, Victor Ramos[1], Gabriela S. Santos[1], Thomas Hägglöf[1], Christian T. Mayer[2], Brianna Hernandez[1], Anna Gazumyan[1], Michel C. Nussenzweig[1,3]*

Increased antibody affinity over time after vaccination, known as affinity maturation, is a prototypical feature of immune responses. Recent studies have shown that a diverse collection of B cells, producing antibodies with a wide spectrum of different affinities, is selected into the plasma cell (PC) pathway. How affinity-permissive selection enables PC affinity maturation remains unknown. We found that PC precursors (prePCs) expressing high-affinity antibodies received higher levels of T follicular helper cell (T_{FH} cell)–derived help and divided at higher rates compared with their lower-affinity counterparts once they left the germinal center. Our findings indicate that differential cell division by selected prePCs accounts for how diverse precursors develop into a PC compartment that mediates serological affinity maturation.

Increasing antibody affinity over time after vaccination is a prototypical feature of humoral immune responses. Experiments in transgenic mice suggest that in the early germinal center (GC)–independent stages of the immune response, B cells expressing high-affinity B cell receptors are preferentially selected into the plasma cell (PC) compartment (1–3).

Selection within the GC reaction itself is governed by T follicular helper cells (T_{FH} cells) that recruit B cells and control the degree of B cell clonal expansion (4). B cells expressing receptors that bind to and can capture antigen displayed on the surface of follicular dendritic cells in the light zone (LZ) process and present antigens to a limited number of T_{FH} cells in exchange for help signals. Selected LZ B cells initiate a transcriptional program that enables them to move into the dark zone (DZ), where they undergo division and somatic mutation before returning to the LZ to test their newly mutated receptors in subsequent rounds of selection. The number of division cycles and the speed of cell division in the DZ is directly related to the strength of T_{FH} cell signals and is governed by the level of *Myc* expression (5–7). Iterative cycles of DZ division and LZ selection produce GC B cells with increasing affinity for the immunogen over the course of an immune response. However, loss of affinity owing to persistent somatic mutation and evolution of the T_{FH} cell compartment eventually leads to GC diversification and increasing inclusion of lower-affinity B cells (8–12).

High-affinity cells of GC origin become enriched in the antibody-secreting PC compartment over time after immunization (13–16). This observation, in conjunction with the known selection mechanisms within the GC, originally supported a model whereby high-affinity cells preferentially undergo PC differentiation. In contrast to these findings, three recent independent studies have shown that in genetically intact animals, diverse collections of GC B cells develop into PC progenitors (8, 17, 18). Additionally, these studies found little or no enrichment for high-affinity antibody–expressing cells among the precursor population, PC precursors (prePCs) (19, 20), in the GC (8, 17, 18). How this population of GC precursors that expresses antibodies with a broad range of affinities gives rise to a PC compartment dominated by cells producing high-affinity antibodies is not understood.

High-affinity cells are overrepresented in the PC compartment

To examine the relationship between GC B cells and PCs, we tracked the two cell types using fate mapping of S1pr2-CreERT2 R26$^{lsl-ZSGreen}$ mice in which tamoxifen administration permanently labels GC cells and their subsequent products (21). Administration of tamoxifen to immunized mice confirmed that this reporter strain labels GC B cells and activated B cells but not mature PCs (fig. S1, A to C). Tamoxifen was administered 5 days after immunization with the model hapten antigen 4-hydroxy-3-nitrophenyl (NP) conjugated to the carrier protein ovalbumin (OVA) (NP-OVA), and single-cell sequencing was performed on labeled GC B cells and PCs isolated from the draining lymph node on day 14 (Fig. 1, A and B). Uniform manifold approximation and projection (UMAP) integrating cellular indexing of transcriptomes and epitopes by sequencing (CITE-seq) data revealed distinct clusters of GC B cells and PCs characterized by Fas and CD86 or by

CD138 surface protein expression, respectively (fig. S2).

Immunoglobulin (Ig) sequence analysis showed expanded clones of cells that were further subdivided into nodes containing one or more cells expressing identical antibodies. The combined clonal trees consisted of 535 individual nodes with 1 to >100 members (Fig. 1C). On the basis of surface staining and gene expression profiles, nodes were divided into those consisting of only GC B cells, both GC B cells and PCs ("mixed nodes"), or only PCs. Nodes consisting of only PCs were the least abundant, representing <8% of the nodes (38 of 535 nodes; Fig. 1D). Most PCs were found within mixed nodes that were also larger than either GC- or PC-only nodes (Fig. 1, E to G). IGHV1-72 antibody expression is associated with relatively high-affinity NP binding (22). Notably, compared with GC nodes, nodes containing PCs were enriched for affinity-enhancing mutations in IGHV1-72 [W33L (i.e., Trp^{33}→Leu), K59R (Lys^{59}→Arg), or Y99G (Tyr^{99}→Gly)] (22, 23) (Fig. 1H). Furthermore, irrespective of node identity, PCs were enriched for affinity-enhancing mutations compared with contemporaneously labeled GC B cells (63 ± 23% PC versus 42 ± 11% GC; P = 0.02; Fig. 1I). Thus, although prePC antibody affinity is indistinguishable from contemporaneous GC B cells (8, 17, 18), PCs are enriched for high-affinity antibodies. Moreover, the presence of identical antibody sequences in large, expanded nodes containing GC B cells and PCs suggests that the mechanisms that govern clonal expansion of the two cell types overlap.

Differential expansion of high-affinity PCs

Two nonexclusive cellular processes could contribute to the observed enrichment of high-affinity PCs over GC B cells: differential cell death and/or division. To determine whether cell death contributed to PC affinity maturation, we purified live and dying PCs from draining lymph nodes of NP-OVA–immunized mice using the Rosa26$^{INDIA/INDIA}$ apoptosis reporter mice (24). Ig sequence analysis revealed similar abundance of high-affinity IGHV1-72–expressing cells in live and dying PC fractions (fig. S3, A to D). In addition, most Ig sequences found among apoptotic PC clones were also present in the live fraction (fig. S3C). Thus, differential cell death did not appear to drive the accumulation of high-affinity PCs over time.

To determine whether high-affinity PCs have a proliferative advantage, we tracked cell division using Vav^{tTa} Col1A1-tetO-histone H2B^{mCherry} reporter mice (H2B-mCherry) (25). Under steady-state conditions, tTA is expressed in hematopoietic cells and induces high levels of the histone H2B-mCherry fusion protein expression. Administration of doxycycline represses histone H2B-mCherry synthesis, and therefore mCherry fluorescence dilutes in

[1]Laboratory of Molecular Immunology, The Rockefeller University, New York, NY, USA. [2]Experimental Immunology Branch, Center for Cancer Research, National Cancer Institute, National Institutes of Health, Bethesda, MD, USA. [3]Howard Hughes Medical Institute (HHMI), The Rockefeller University, New York, NY, USA.
*Corresponding author. Email: nussen@rockefeller.edu (M.C.N.); amaclean@rockefeller.edu (A.J.M.)
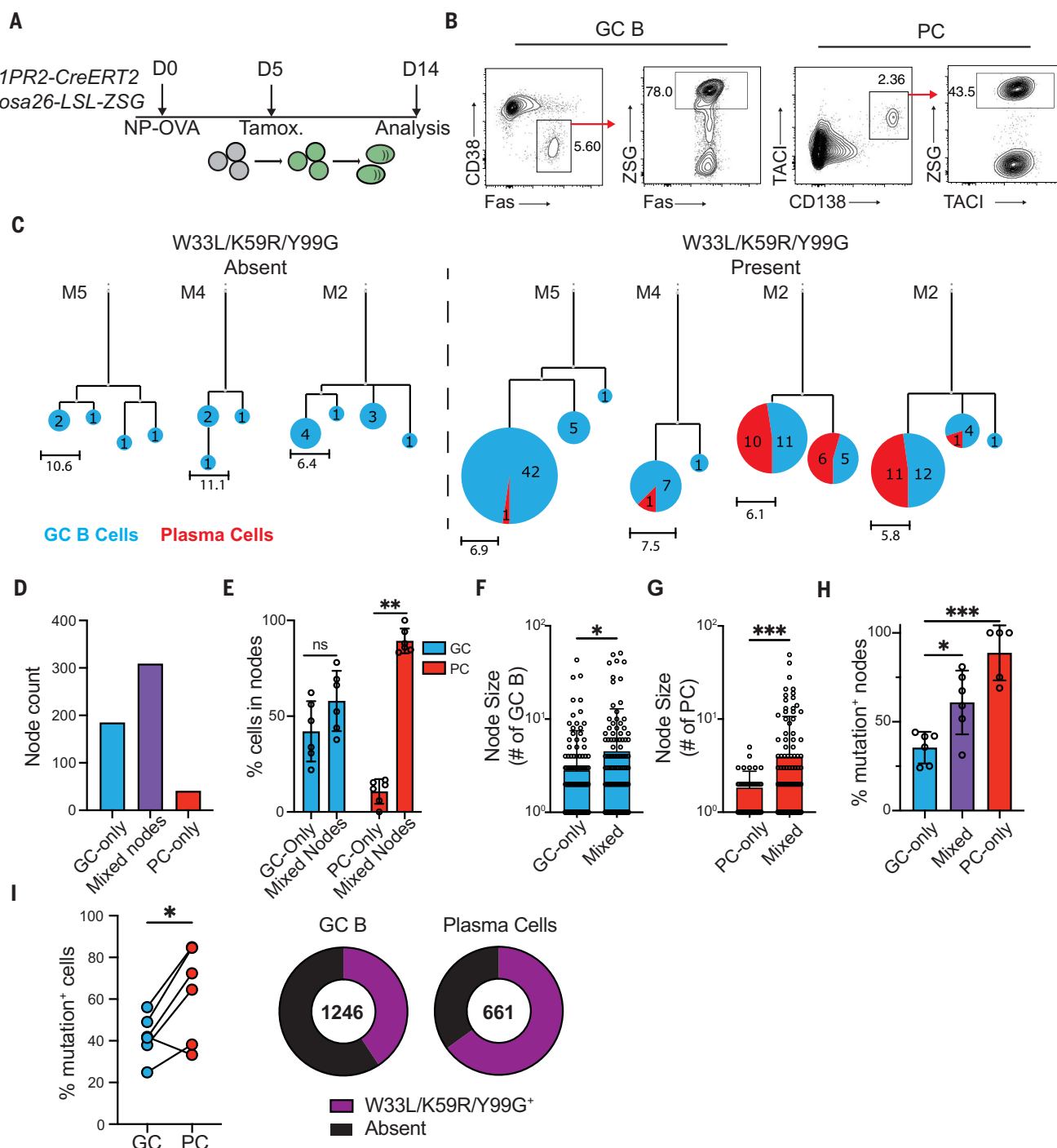†Present address: Department of Immunology, Harvard Medical School, Boston, MA, USA.

Fig. 1. High-affinity antibody–producing PCs are overrepresented relative to contemporaneous GC B cells. (**A**) Experimental layout for (B) to (H). D0, day 0; Tamox., tamoxifen. (**B**) Representative flow cytometry plots showing strategy for isolating popliteal lymph node (pLN) GC B cells (pregated on live, TACI⁻ CD138⁻ B220⁺; CD38⁻Fas⁺ZSG⁺) and PCs (pregated on live; CD138⁺TACI⁺ZSG⁺). Full gating strategy is displayed in fig. S2A. (**C**) Representative IgH+IgL sequence-based phylogenetic trees highlighting GC B cell (blue) and PC (red) distribution. Expanded clones containing (right) or not containing (left) affinity-enhancing mutations. Each circle represents one node of cells with identical sequences. Scale represents mutational distance observed between related sequences. (**D**) Total numbers of GC-only, PC-only, or mixed nodes analyzed. (**E**) Frequency of GC B cells (blue bars)

or PCs (red bars) found within mixed or single-cell–type nodes. Each point represents one animal. (**F** and **G**) Node size: Number of individual GC B cells (F) or PCs (G) in either uniform or mixed nodes. (**H**) Frequency of nodes with affinity-enhancing mutations. Each point represents one mouse, summarizing 51 to 176 nodes per mouse. (**I**) Frequency of affinity-enhancing mutations within total GC B cells and PCs. (Left) Summary. Each pair of connected points represents GC B cells and PCs isolated from one animal. (Right) Quantitation of total cells. Numbers in center represent total number of sequences analyzed. *$P < 0.05$; **$P < 0.005$; ***$P < 0.0005$; ns, not significant. Statistics by analysis of variance (ANOVA) [(F) and (G)], mixed effects analysis (H), or paired two-tailed Student's t test (I). Data are pooled from two independent experiments, $n = 6$ mice per group.
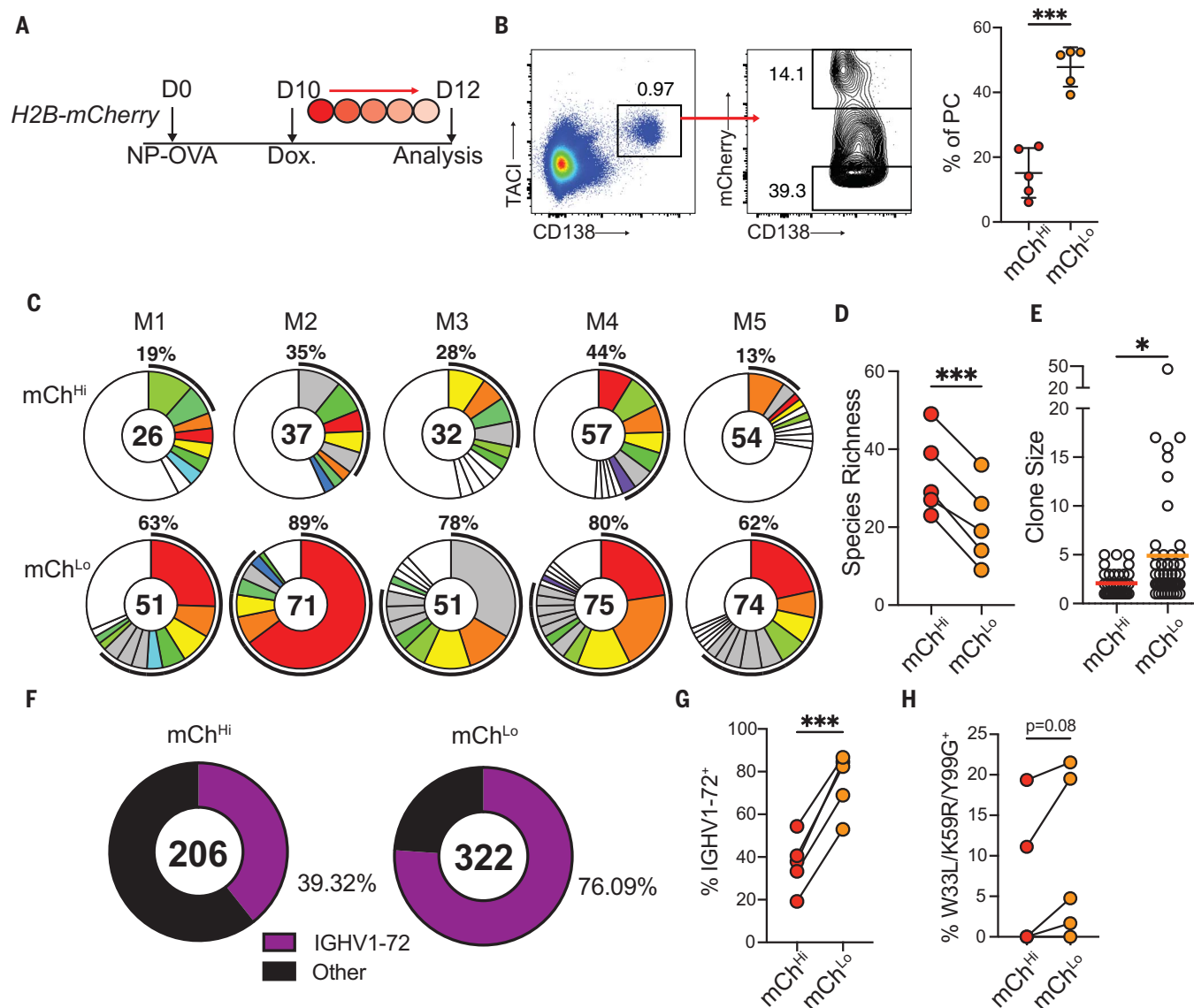
Fig. 2. High-affinity antibody–producing PCs are more proliferative. (A) Experimental layout for (B) to (F). Dox., doxycycline. **(B)** (Left) Flow cytometry profile showing TACI⁺CD138⁺ PCs and gating for mCherryʰⁱ (mChʰⁱ) and mCherryˡᵒ (mChˡᵒ) cells from pLNs. (Right) mChˡᵒ and mChʰⁱ PC frequency. Each point represents one mouse. Graphs display means ± SDs. **(C)** Clonal distribution of paired Ig sequences (IgH+IgK/IgL) among mChʰⁱ and mChˡᵒ PCs isolated from each mouse. Colored segments represent expanded clones, and singlets are represented by white segments. The number in the center represents the number of sequences analyzed per population. The outer segment annotation denotes the percentage of cells that are members of expanded clones. **(D)** Chao1 species richness quantification. Each pair of points represents one mouse. **(E)** Clone size. Each point represents one clone. **(F)** Frequency of mChʰⁱ or mChˡᵒ PCs bearing high-affinity IGHV1-72 B cell receptors. Number in center represents total number of sequences. **(G)** Summary of (F). Each pair of points represents one mouse. **(H)** Frequency of high-affinity mutation–containing sequences among IGHV1-72⁺–expressing mChʰⁱ or mChˡᵒ PCs. *$P < 0.05$; ***$P < 0.0005$. Statistics by paired two-tailed Student's t test [(B), (D), (G), and (H)] or unpaired Student's t test (E). Data are pooled from two independent experiments, $n = 5$ mice per group.

proportion to cell division (25). H2B-mCherry mice were immunized with NP-OVA and were administered doxycycline 10 days after immunization. PCs were isolated from draining lymph nodes 2 days later on the basis of their high or low levels of division (mCherryˡᵒ and mCherryʰⁱ PCs, respectively; Fig. 2, A and B). mCherryˡᵒ PCs that had undergone greater levels of division showed reduced species richness and larger clonal families when compared with their non-dividing counterparts, indicating rapid clonal expansion in this population (Fig. 2, C to E). Notably, there was an enrichment of PCs expressing high-affinity IGHV1-72 among the more divided PCs (75.1 ± 14% mCherryˡᵒ versus 37.1 ± 12% mCherryʰⁱ; $P = 0.0001$; Fig. 2, F and G). At this early time point, the W33L, K59R, and/or Y99G affinity-enhancing mutations were largely absent from both IgHV1-72⁺ PC populations, but there was a trend toward enrichment in the more divided mCherryˡᵒ group (Fig. 2H; $P = 0.08$). These findings were confirmed using Blimp1-CreERT2 R26ˡˢˡ⁻ᶻˢGreen mice, a reporter strain that selectively labels differentiated PCs (fig. S4, A and B). Blimp1-CreERT2 R26ˡˢˡ⁻ᶻˢGreen mice were combined with H2B-mCherry mice to enable tamoxifen-mediated ZsGreen (ZSG) labeling of a synchronized cohort of PCs, which can be division tracked by mCherry dilution. Isolation of mCherryʰⁱ and mCherryˡᵒ ZSG⁺ PCs revealed that among mature PCs, the more proliferative cells were enriched for NP bait binding and expression

Fig. 3. Post-GC expansion of PCs. (**A** and **B**) Confocal microscopy images of pLNs isolated from S1pr2-CreERT2 R26$^{lsl-ZSGreen}$ mice immunized with NP-OVA, treated with tamoxifen on D8 and anti-CD40L or isotype control on D10 and D12. Large tiles show overview of pLN architecture. Inset boxes show individual clusters of dividing Ki67$^+$ NP$^+$ PCs that are highlighted by dashed circles. Individual channels are shown beside merged images. Scale bars, 100 μm (large tiles) and 30 μm (inset boxes). Ctrl, control. (**C**) Quantitation of fraction of medullary PCs that are Ki67$^+$ among NP$^+$ and NP$^-$ populations, as quantified from confocal images, as in (A). The number in the center represents the number of cells analyzed per population. (**D**) Summary of (C). Each point represents one mouse. Graph displays means ± SDs. *$P < 0.05$; **$P < 0.005$; ordinary one-way ANOVA. Data are representative of three experiments, $n = 3$ to 4 mice per group.
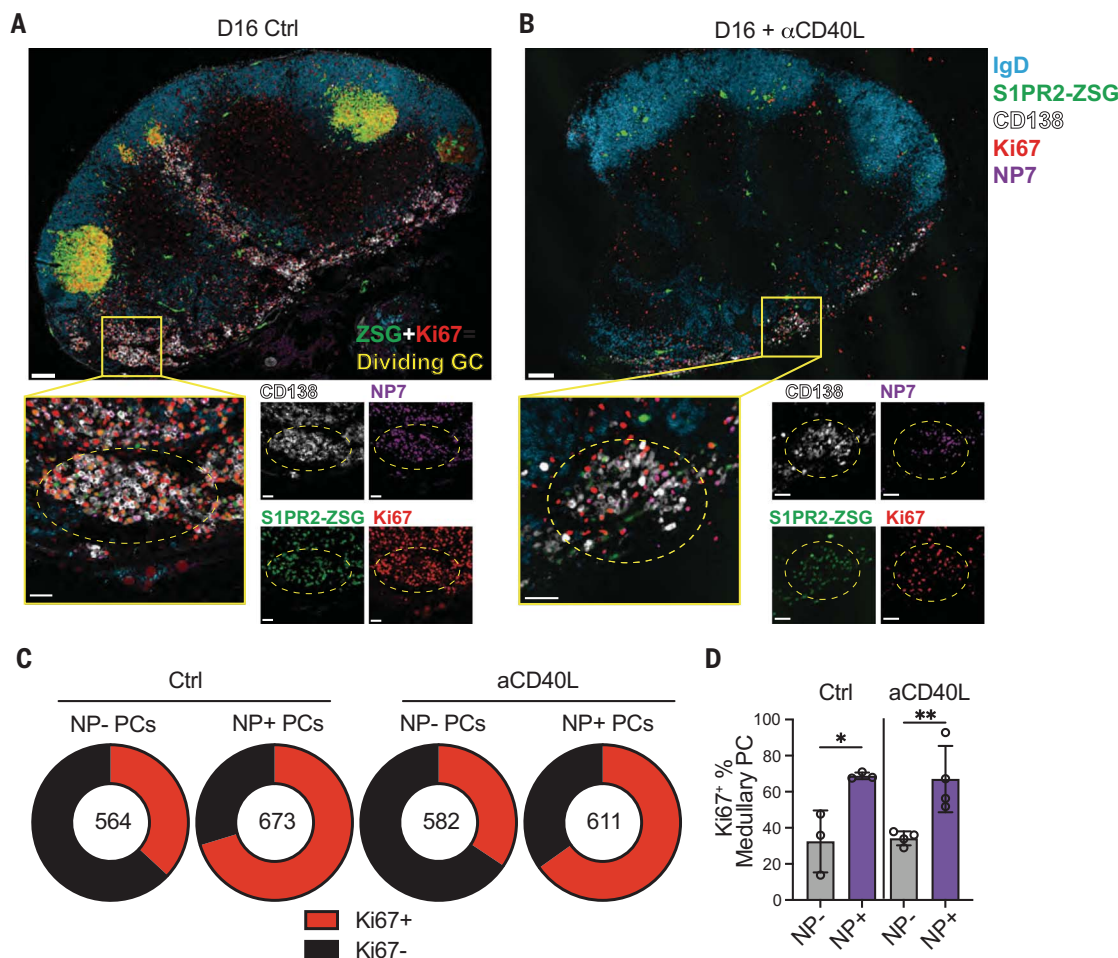
of high-affinity Ig gene rearrangements (fig. S4, C to H). These data indicated that higher-affinity B cell receptor expression was associated with differential division at the mature PC stage.

To validate these findings using vaccine antigens, we immunized H2B-mCherry mice with either severe acute respiratory syndrome coronavirus 2 (SARS-CoV-2) receptor binding domain (RBD) or combined tetanus and diphtheria toxoid antigens (Tenivac) and administered doxycycline on day 10 after vaccination. Antigen binding was used as a surrogate for higher-affinity antigen binding cells (fig. S5, A and B). Flow cytometric analysis revealed that RBD or tetanus and diphtheria toxoid binding cells were enriched and showed higher mean fluorescence among the divided mCherry^{lo} compared with mCherry^{hi} cells, even when normalized for surface Ig expression levels (fig. S5, C to H). The combined dataset indicated that high-affinity PCs underwent greater levels of clonal expansion than lower-affinity PCs irrespective of the composition of the administered immunogen or adjuvant formulation.

PC selection outside of the GC

To examine the site of affinity-driven PC clonal expansion, S1pr2-CreERT2 R26$^{lsl-ZSGreen}$ mice were immunized with NP-OVA, treated with tamoxifen on day 8, and then given anti-CD40L or isotype control antibodies on days 10 and 12 after immunization. In this setting, tamoxifen will label GC products and anti-CD40L will terminate the GC reaction 2 days later, allowing a cohort of PCs generated between days 8 and 10 to be tracked. Draining lymph nodes were examined by confocal microscopy on day 16 after immunization (Fig. 3, A and B, and fig. S6A).

Large GCs, in which many of the cells were actively dividing (as determined by positive staining for Ki67), were observed in control mice that did not receive anti-CD40L. In addition, we found discrete clusters of dividing NP-binding PCs (marked by CD138$^+$ZSG$^+$Ki67$^+$NP$^+$) that were particularly abundant in the lymph node medulla. Anti-CD40L treatment aborted the GC reaction (Fig. 3, A and B, and fig. S6, A and B). By contrast, the clusters of proliferating NP-specific PCs persisted (Fig. 3, A and B). Quantitation of medullary PC di-

vision by Ki67 staining revealed a higher proportion of dividing NP-binding PCs than nonbinding PCs. Moreover, this feature was retained on anti-CD40L treatment and GC depletion (Fig. 3, C and D). Thus, dividing antigen-specific PCs were observed in medullary foci outside of the anatomical confines of the GC, and these foci were maintained in the absence of active GCs during the observation period.

To determine whether the observed enrichment of high-affinity PCs continued in a post-GC compartment, we isolated PCs from anti-CD40L–treated S1pr2-CreERT2 R26$^{lsl-ZSGreen}$ mice. The mice also received the drug FTY720 to inhibit S1PR1-driven egress signals and to prevent PCs from leaving the node (26). Treatment with anti-CD40L effectively depleted draining lymph nodes of GCs and activated B cells within 2 days (Fig. 3, A and B, and fig. S6, A to D). Ig sequence analysis on day 10 showed that 67% of labeled PCs were IGHV1-72$^+$ and that by day 16, this increased to 83% under control conditions ($P = 0.037$; Fig. 4, A to E). Notably, the PC compartment was equally enriched for high-affinity clones on day 16 in
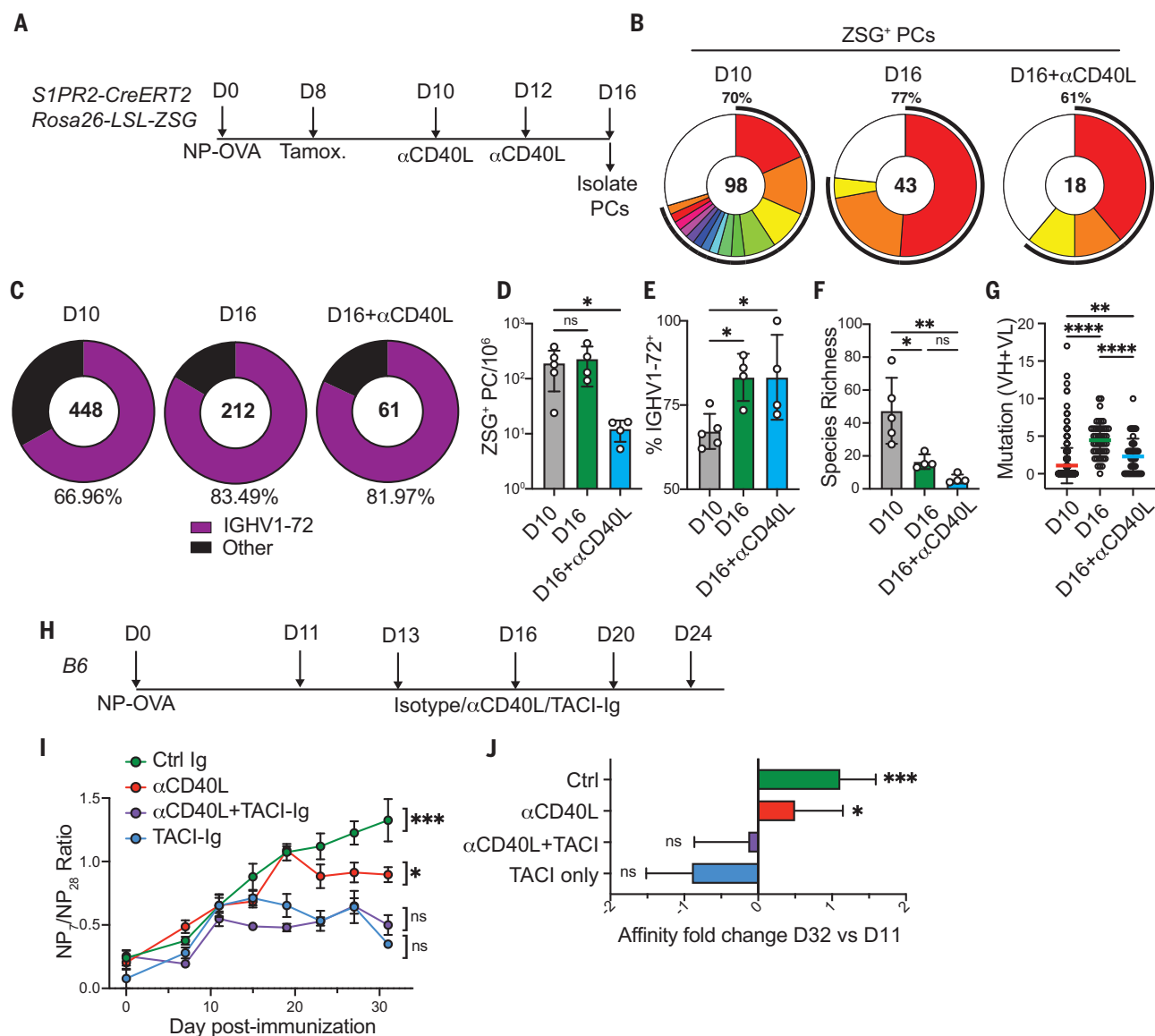
Fig. 4. Post-GC evolution of the PC repertoire and serological affinity maturation. (**A**) Experimental layout for (B) to (G). (**B**) Clonal distribution of paired Ig sequences from representative mice. Colored segments represent expanded clones, and singlets are represented by white segments. The number in the center represents the number of sequences analyzed per population. The outer segment annotation denotes the percentage of cells that are members of expanded clones. (**C**) Frequency of ZSG+ PCs expressing IGHV1-72. The number in the center represents the number of sequences analyzed. (**D**) Number of ZSG+ PCs in each experimental group. (**E**) Summary of IGHV1-72 frequency presented in (C). (**F**) Chao1 species richness. In (D) to (F), each point represents one mouse, n = 4 to 5 mice per condition. (**G**) Number of VH+VL mutations in paired Ig sequences. Each point represents one cell. (**H**) Experimental layout for (I) and (J). (**I**) Ratio of NP_7/NP_{28}-binding IgG in serum measured by enzyme-linked immunosorbent assay (ELISA). (**J**) Fold change in affinity (NP_7/NP_{28} ratio) at D32 versus D11. Data are presented as means ± SDs. Data are representative of two experiments, n = 5 to 10 mice per group. *$P < 0.05$; **$P < 0.005$; ****$P < 0.0001$. Statistics by ordinary one-way ANOVA [(D) to (F)], Kruskal-Wallis test (G), or mixed effects analysis [(I) and (J)]. For full statistical comparisons, see fig. S4E.

mice treated with anti-CD40L under conditions that depleted GCs (Fig. 4, C to E). In addition, the PC compartment in CD40L-treated mice displayed the same characteristic reduction in species richness that was indicative of clonal expansion seen in control mice (Fig. 4, B and F). Finally, labeled PCs obtained from anti-CD40L–treated mice displayed a reduced mutational load, which suggests that they

were derived from GC precursors that exited the GC at a time when mutations were less abundant (Fig. 4G).

Serological affinity maturation is typified by a rapid increase in the affinity of circulating antibodies (*27*). We hypothesized that the continued preferential expansion of high-affinity PCs after GC depletion (Fig. 4, A to G) would lead to measurable improvements in serum

anti-NP affinity. To determine whether PCs in anti-CD40L–treated mice continue to support affinity maturation after depletion of GC and activated B cells, we measured the serum antibody binding to bovine serum albumin derivatized with either 7 or 28 molecules of NP (Fig. 4H and fig. S6, A to E). Control mice displayed a marked increase in NP_7/NP_{28} immunoglobulin G (IgG) binding ratio between days 12 and 32,

Fig. 5. PC proliferation is proportional to signal strength. (**A**) Experimental outline for (B) to (F). i.p., intraperitoneal; ko, knockout. (**B**) Representative flow cytometry plots showing GC B cells (B220$^+$CD38$^-$Fas$^+$; top) and prePCs (B220$^+$CD38$^-$Fas$^+$CD138$^+$; bottom) after treatment with different ratios of anti–DEC-205–OVA:CS. (**C** and **D**) Quantitation of DEC^{WT} (WT, wild-type) GC B cells (C) and prePCs (D) 24 hours after anti–DEC-205 treatment. (**E** and **F**) Quantitative polymerase chain reaction (qPCR) of sorted DEC^{WT} GC LZ (CD86$^+$CXCR4$^-$ GC B cells) and prePCs (as above), showing glyceraldehyde-3-phosphate dehydrogenase (GAPDH)–normalized relative expression for *Myc* (E) and *Tfap4* (F). Data in (A) to (D) and (E) and (F) are representative of three independent experiments, *n* = 6 to 8 mice per group. (**G**) Experimental outline for (H) to (K). (**H** and **I**) Quantitation of DEC^{WT} GC B cells (H) and Ki67$^+$ DEC^{WT} GC B cells (I). (**J** and **K**) Quantitation of DEC^{WT} PCs (J) and Ki67$^+$ DEC^{WT} PCs (K). Data are presented as means ± SDs. Each point in (C), (D), and (H) to (K) represents one mouse. Data in (H) to (K) are representative of four independent experiments. *$P < 0.05$; **$P < 0.005$; ***$P < 0.0005$. Statistics by ANOVA (C) or Kruskal-Wallis test [(D) and (H) to (K)].
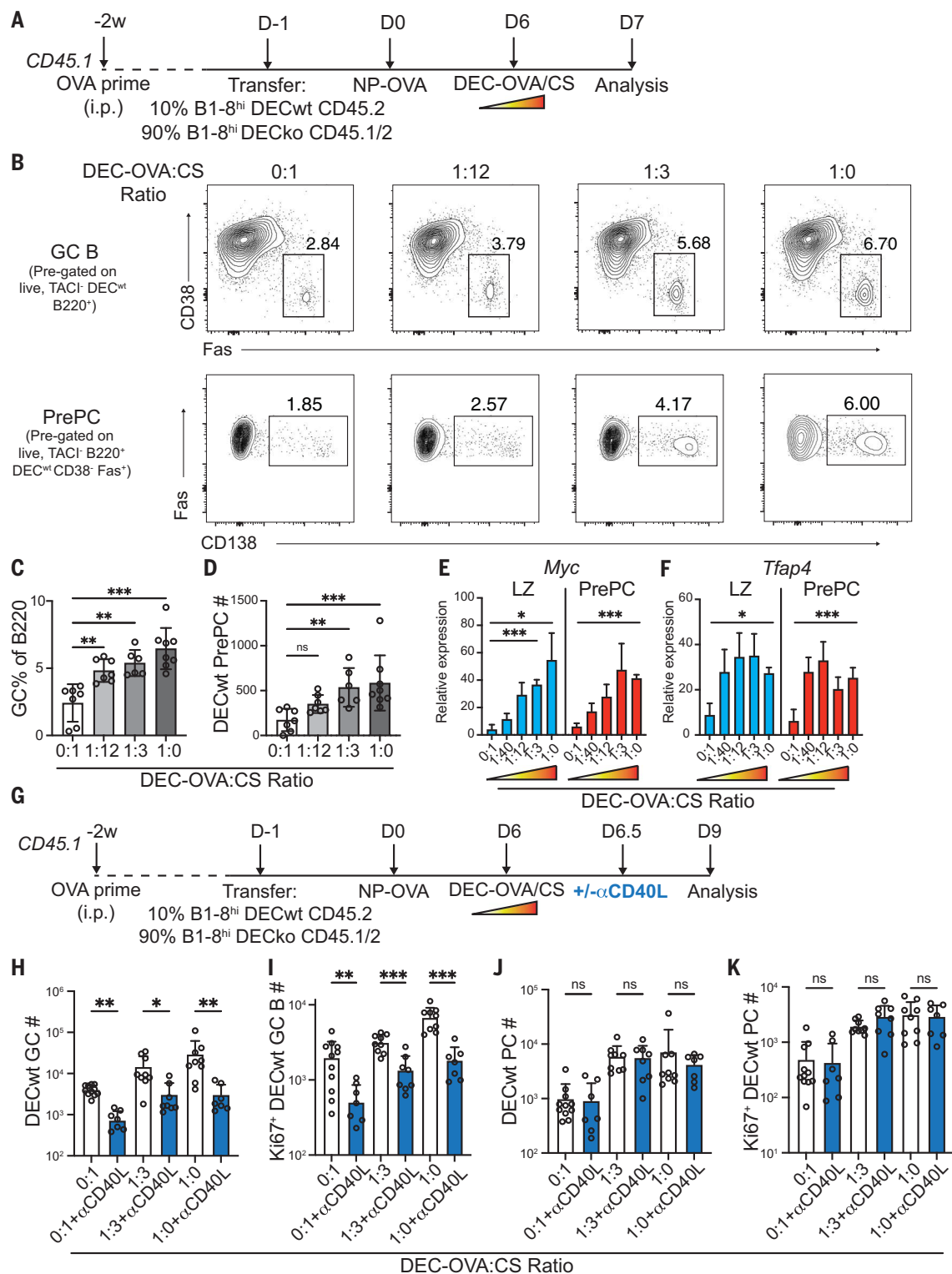
indicating a rapid increase in anti-NP affinity that was aborted by depleting PCs with TACI-Ig (Fig. 4I). Notably, and consistent with the above sequencing data, the serum antibody response continued to undergo affinity maturation for several weeks after anti-CD40L treatment (Fig. 4, I and J).

We concluded that serological affinity maturation can proceed in the absence of continued output from the GC reaction, and it was suppressed by PC depletion. These findings suggest that after export from the GC, newly generated PCs undergo affinity-based expansion in a manner that contributes to increasing serum antibody affinity.

PC division is proportional to the strength of T cell help

GC B cells in the LZ of the GC structure compete for limited help signals from T$_{FH}$ cells, a process known as positive selection. The amount of help received by a B cell is directly proportional to the amount of antigen captured and

presented by the B cell (*25, 28*). Positively selected GC B cells up-regulate expression of the transcription factor *Myc* in proportion to the strength of T cell signals and migrate to the DZ, where they undergo cycles of T_{FH} cell–independent inertial cell division in proportion to the amount of *Myc* expression (*5, 25, 29*).

To determine whether a similar process regulates the relative amount of PC expansion, we delivered graded doses of the antigen OVA to ongoing GCs using chimeric anti–DEC-205–OVA antibodies (*28*) (Fig. 5A). Protein antigens loaded onto anti–DEC-205 are delivered to DEC-205$^+$ GC B cells, supplying a B cell receptor–independent supply of antigen that can be processed and presented to T_{FH} cells (*28*). As expected, GC B cells expanded in direct proportion to the amount of antigen delivered (Fig. 5, B and C). Antigen delivery by anti–DEC-205–OVA also produced a rapid increase in the frequency and numbers of prePCs (B220^{hi} CD38$^-$ Fas$^+$ CD138$^+$; Fig. 5, B and D). To determine whether prePCs in the LZ of the GC also expressed *Myc* in proportion to antigen delivery by DEC-205, we purified these cells 24 hours after graded doses of anti–DEC-205–OVA injection. Consistent with their commitment to the PC fate, these cells displayed elevated levels of *Irf4*, a transcription factor that promotes PC differentiation, and lower expression levels of the antigen receptor signaling-induced factor *Nr4a1* compared with other LZ GC B cells (fig. S7, A and B). Notably, they showed increases in *Myc* that were directly proportional to the amount of antigen delivered (Fig. 5E). *Tfap4*, a transcription factor downstream of c-Myc, also showed a similar induction pattern, although the expression of this factor plateaued at lower antigen concentrations (Fig. 5F). In addition, prePC proliferation, as measured by Ki67 expression, was proportional to the amount of antigen supplied (fig. S7, C and D).

To test whether T_{FH} cell help in the LZ could support continued PC expansion, anti-CD40L was administered 12 hours after anti–DEC-205–OVA. In this setting, GC B cells acquired high levels of cognate antigen and interacted with T_{FH} cells for ~12 hours, after which subsequent T cell help was inhibited by CD40L blockade as evidenced by GC collapse (Fig. 5G; Fig. 3, A and B; and fig. S6, A and B). Treatment with anti-CD40L 12 hours after anti–DEC-205–OVA injection prevented further GC B cell expansion and blocked additional Ki67 expression in GC B cells, including prePCs (Fig. 5, H and I, and fig. S7, E and F). By contrast, mature PCs continued to expand and divide in the days after anti-CD40L treatment in direct proportion to the amount of antigen captured (Fig. 5, J and K). The data indicated that after a short pulse of T cell help, developing prePCs up-regulated *Myc* and underwent cycles of cell division in the absence of continued T cell signals.

Other signals are known to enhance the magnitude of the PC response (*14*). For example, PCs are highly sensitive to the levels of the cytokine interleukin-21 (IL-21) (*30, 31*), and IL-21–producing T cells have been reported to localize in foci outside of the B cell follicle (*32*). To test whether IL-21 could support the expansion of committed PCs, we fate mapped PCs on day 8 using Blimp1-CreERT2 reporter mice and subsequently treated with anti-CD40L or anti–IL-21R from days 10 to 12. PC division was assessed by Ki67 staining. As expected, analysis of ZSG-labeled PCs revealed that continued CD40L signals were not required to sustain PC proliferation (fig. S8, A to C). By contrast, partial blockade of IL-21R led to reduced proliferation of mature ZSG$^+$ PCs, which indicates that IL-21 supports the post-GC expansion of PCs (fig. S8, B and C).

Discussion

Current models of PC differentiation suggest that B cell receptor affinity is deterministic of cell fate (*14, 15, 27*). Our experiments indicated that although a heterogeneous collection of prePCs—including those expressing low-affinity receptors—developed into PCs, they subsequently underwent differential affinity-dependent division. As a result, PCs expressing higher-affinity antibodies contributed disproportionately to serum antibodies, promoting affinity maturation.

Antibody responses develop in two stages: a GC-independent early phase during which B cells rapidly develop into dividing plasmablasts that produce relatively lower-affinity antibodies and a second GC-dependent phase that produces higher-affinity antibodies responsible for serologic affinity maturation. In transgenic mice that carry high-affinity antibodies, the early GC-independent rapid burst of PC development and expansion is affinity dependent (*1, 2*). By contrast, under physiologic circumstances, this early PC response produces primarily germline-encoded antibodies with relatively lower affinity compared with those produced in GCs (*15, 33, 34*). In animals with a polyclonal B cell repertoire, GCs enable B cell clonal expansion and antibody hypermutation, both of which are essential for antibody affinity maturation (*27, 35, 36*). Our experiments elucidated the mechanisms by which GC-dependent PC selection enables affinity maturation in polyclonal immune responses.

The GC LZ also contains prePCs that express IRF4, CD138, and variable levels of Myc and share many of the transcriptional features of LZ B cells selected for DZ reentry (*8, 14*). Similar to DZ B cells, PC descendants of prePCs undergo rapid cell division in GC-adjacent sites, but they do not undergo additional somatic mutation and so retain antibody specificity (*37*). Our experiments show that the amount of clonal expansion by newly exported PCs

was directly proportional to affinity and the strength of historic selection signals that these cells received in the LZ, providing a mechanistic explanation for how PC selection is regulated in relation to affinity. Notably, our data are entirely consistent with the observation that the PC pool tends to be more clonal than the contemporary GC B cells or prePCs from which they develop (*8, 17*). In addition to PCs in the lymph nodes, long-lived PCs in the bone marrow are also enriched for high-affinity antibody–producing cells (*38, 39*). Our data suggest that this phenomenon is likely a result of overrepresentation of high-affinity PCs among dividing plasmablasts that subsequently seed the bone marrow.

Post-GC PC clonal expansion in proportion to historical T_{FH} cell signals and *Myc* expression parallels Myc-regulated GC B cell clonal expansion, thereby enabling rapid affinity maturation. The proposed model does not preclude permissive selection of GC cells with diverse affinities into the PC compartment (*8, 17, 18*). Instead, our findings help resolve the apparent contradiction between affinity-permissive selection into the PC compartment and rapid affinity maturation.

REFERENCES AND NOTES

1. D. Paus *et al.*, *J. Exp. Med.* **203**, 1081–1091 (2006).
2. T. D. Chan *et al.*, *J. Immunol.* **183**, 3139–3149 (2009).
3. T. G. Phan *et al.*, *J. Exp. Med.* **203**, 2419–2424 (2006).
4. S. Crotty, *Immunity* **50**, 1132–1148 (2019).
5. S. Finkin, H. Hartweger, T. Y. Oliveira, E. E. Kara, M. C. Nussenzweig, *Immunity* **51**, 324–336.e5 (2019).
6. D. Dominguez-Sola *et al.*, *Nat. Immunol.* **13**, 1083–1091 (2012).
7. D. P. Calado *et al.*, *Nat. Immunol.* **13**, 1092–1100 (2012).
8. M. A. ElTanbouly *et al.*, *J. Exp. Med.* **221**, e20231838 (2024).
9. T. Hägglöf *et al.*, *Cell* **186**, 147–161.e15 (2023).
10. R. V. H. de Carvalho *et al.*, *Cell* **186**, 131–146.e13 (2023).
11. J. Merkenschlager *et al.*, *Nature* **591**, 458–463 (2021).
12. J. Merkenschlager *et al.*, *Nat. Commun.* **14**, 6944 (2023).
13. T.-A. Yang Shih, E. Meffre, M. Roederer, M. C. Nussenzweig, *Nat. Immunol.* **3**, 570–575 (2002).
14. W. Ise, T. Kurosaki, *Immunol. Rev.* **288**, 64–74 (2019).
15. S. L. Nutt, P. D. Hodgkin, D. M. Tarlinton, L. M. Corcoran, *Nat. Rev. Immunol.* **15**, 160–171 (2015).
16. A. Radbruch *et al.*, *Nat. Rev. Immunol.* **6**, 741–750 (2006).
17. A. Sprumont, A. Rodrigues, S. J. McGowan, C. Bannard, O. Bannard, *Cell* **186**, 5486–5499.e13 (2023).
18. H. J. Sutton *et al.*, *Immunity* **57**, 245–255.e5 (2024).
19. W. Ise *et al.*, *Immunity* **48**, 702–715.e4 (2018).
20. N. J. Kräutler *et al.*, *J. Exp. Med.* **214**, 1259–1267 (2017).
21. R. Shinnakasu *et al.*, *Nat. Immunol.* **17**, 861–869 (2016).
22. D. Allen, T. Simon, F. Sablitzky, K. Rajewsky, A. Cumano, *EMBO J.* **7**, 1995–2001 (1988).
23. K. Furukawa, A. Akasako-Furukawa, H. Shirai, H. Nakamura, T. Azuma, *Immunity* **11**, 329–338 (1999).
24. C. T. Mayer *et al.*, *Science* **358**, eaao2602 (2017).
25. A. D. Gitlin, Z. Shulman, M. C. Nussenzweig, *Nature* **509**, 637–640 (2014).
26. K. Kabashima *et al.*, *J. Exp. Med.* **203**, 2683–2690 (2006).
27. G. D. Victora, M. C. Nussenzweig, *Annu. Rev. Immunol.* **40**, 413–442 (2022).
28. G. D. Victora *et al.*, *Cell* **143**, 592–605 (2010).
29. J. Pae *et al.*, *J. Exp. Med.* **218**, e20201699 (2021).
30. Z. Chen *et al.*, *Sci. Immunol.* **8**, eadd1728 (2023).
31. K. Ozaki *et al.*, *J. Immunol.* **173**, 5361–5371 (2004).
32. J. M. Odegard *et al.*, *J. Exp. Med.* **205**, 2873–2886 (2008).
33. I. C. MacLennan *et al.*, *Immunol. Rev.* **194**, 8–18 (2003).
34. J. G. Cyster, C. D. C. Allen, *Cell* **177**, 524–540 (2019).
35. N. S. De Silva, U. Klein, *Nat. Rev. Immunol.* **15**, 137–148 (2015).
36. J. Jacob, G. Kelsoe, K. Rajewsky, U. Weiss, *Nature* **354**, 389–392 (1991).

37. Y. Zhang *et al.*, *J. Exp. Med.* **215**, 1227–1243 (2018).
38. M. J. Robinson *et al.*, *Sci. Immunol.* **7**, eabm8389 (2022).
39. Y. Takahashi, P. R. Dutta, D. M. Cerasoli, G. Kelsoe, *J. Exp. Med.* **187**, 885–895 (1998).

SUPPLEMENTARY MATERIALS